N2O catalytic decomposition on electrodeposited Rh-based open-cell metallic foams

N2O catalytic decomposition on electrodeposited Rh-based open-cell metallic foams

Phuoc Hoang Hoa,b, Magdalena Jabłońskab,c,∗,1, Regina Palkovitsb,c,∗,1,

Enrique Rodríguez-Castellónd, Francesca Ospitalia, Giuseppe Fornasaria, Angelo Vaccaria,

Patricia Benitoa,∗

a Dipartimento di Chimica Industriale “Toso Montanari”, Università di Bologna, Viale Risorgimento 4, 40136, Bologna, Italy

b Chair of Heterogeneous Catalysis and Chemical Technology, RWTH Aachen University, Worringerweg 2, 52074 Aachen, Germany

c Center for Automotive Catalytic Systems Aachen, RWTH Aachen University, Schinkelstr. 8, 52062 Aachen, Germany

d Departamento de Química Inorgánica, Facultad de Ciencias, Universidad de Málaga, 29071 Málaga, Spain

HIGHLIGHTS

Rh/Mg/Al HT-derived film uniformly coated the surface of the foam.

Comparable catalysts’ activity re- vealed for constant Rh loading in the bed.

Rh3+ served as the active species for deN2O.

GRAPHICALABSTRACT

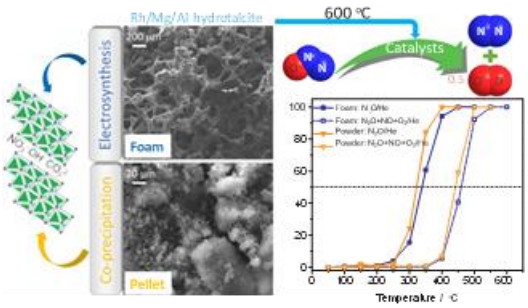

Keywords:

N2O decomposition Hydrotalcite Rhodium Electrodeposition Open-cell foam

A B S T R A C T

The present article reports on Rh-containing hydrotalcite (HT) derived catalysts coated on the surface of open- cell FeCralloy foams. The structured catalysts were prepared by in situ synthesis of Rh/Mg/Al HT precursors through electrodeposition followed by calcination. For comparison purposes, powder catalysts with analogous compositions were obtained by coprecipitation. The catalytic activity in N2O decomposition (deN2O) over structured and pelletized catalysts was investigated in absence and presence of inhibitors (O2 + NO) by keeping similar Rh loading and reaction conditions. Furthermore, stability of the structured catalysts was investigated. A Rh/Mg/Al HT-derived film uniformly coated the surface of the foam. The deN2O performance over both structured and pelletized catalysts was comparable for constant Rh loading in the catalytic bed, though lower activation energy was obtained for the structured catalyst. The coating was stable after a 24 h test at 475 °C in presence of O2 and NO, while rhodium oxide was reduced to Rh0 (2.0 ± 1.1 nm). Due to a low amount of active phase in the thin catalytic coating, the conversion steadily decreased during the first 20 h of time-on-stream from 60 until a constant 51% reaching stable level.

1. Introduction

A significant increase of nitrous oxide (N2O) concentration in the atmosphere lead to global warming and depletion of stratospheric ozone layer [1–3]. Although main sources of N2O are generated by natural processes in lands and oceans, the contributions from anthropogenic sources such as fertilizers, burning of biomass, combustion of fossil fuels, wastewater treatment and industrial activities are also considerable [4]. Depending on the sources of N2O, its abatement could be achieved by either limiting its formation or using end-of-pipe re-mediation technologies (e.g., catalytic decomposition of N2O in adipic acid and nitric acid production). The deN2O technology does not re- quire any reducing reactant of N2O, but active, selective and stable catalyst is mandatory. Noble metal-containing catalysts (especially Rh as one of the most active component) present high activity at relatively low temperatures [4,5]. Rh-bulk catalysts (i.e., perovskites and hydrotalcite derived mixed metal oxides) or Rh supported on oxide supports (e.g., CeO2, TiO2, Al2O3, ZrO2), mesoporous silicas (e.g., SBA-15, KIT-6) or zeolites (e.g., ZSM-5, beta, Y) have been widely investigated [5]. Their activity in deN2O mainly depends on the Rh particle size [6,7] and oxidation state [8,9]. Although, other factors such as support acid- base-redox properties were proved to modify the catalytic properties [8,10–12]. The type of support [6,13], preparation method [14–16], Rh precursor [6,14], and pretreatment conditions [14,17] can alter the Rh particle size.

Hydrotalcite-like (HT) compounds (e.g., Mg-Rh-Al, Co-Rh- Al, Mg-Co-Rh-Al) are well-known catalyst precursors being capable to host Rh3+ with a high dispersion in their structure. After calcination at moderate temperatures (e.g., 400–600 °C) can be decomposed to mixed metal oxides characterized by relatively high specific surface area and small Rh particle size [11,17,18]. Though, the main drawback of Rh- containing catalysts is their high cost being an issue for industrial applications [18].

The decrease in the catalyst particle size can improve its effective-ness. However, generated high pressure-drop (especially at high gas hourly space velocity (GHSV)) may limit the length of the reactor and catalyst mechanical resistance. Structured catalysts, for example based on extruded Fe-ZSM-5 honeycomb monoliths have a high intrinsic activity, high effectiveness and low pressure drop. They can be operated under different requirements of pressure, conversion and high mechanical stability [18]. Also, even if catalyst is only coated on the surface of the monolith. Furthermore, a lower amount of catalyst is required on coated monoliths in comparison to pelletized catalyst in order to obtain comparable activity [19]. For instance, at 500 °C (relatively high operating temperature) the catalyst volume was decreased by one-third, allowing the design of more compact reactors. However, the activity of deN2O structured catalysts strongly depends on the catalyst deposition procedure and its loading (coating). For example, the in situ synthesis of Fe-MOR (mordenite) on cordierite monoliths provided a better accessibility of the zeolite and the prevention (in some extent) of the agglomeration of iron oxides than dip-coating [20]. In the dip-coating, the presence of binder, i.e., silica- or alumina-gel, enhances the performances of Co-BEA or Fe-BEA (beta) monolith samples [21]. When the preparation procedure involves the deposition of the support on the honeycomb followed by impregnation with solution of Rh nitrate, the flash rather than slow calcination generated well distributed Rh particles [22]. Once the preparation procedure was optimized, a comparison between powder and structured catalysts confirmed that the latter have higher reaction rates per gram of catalyst [23–25]. However, in some cases, the increase in the reaction rate may not be sufficient to balance the lower amount of active phase in the coating in comparison with pelletized catalysts [24].

Other types of the supports, such as sintered metal fibers [26] and stainless wire-mesh [27] provided a larger specific surface area for the deposition of Fe-ZSM-5 and K-doped cobalt oxide catalysts, respectively. Open-cell metallic foams provide advantages compared to honeycomb monoliths (larger geometrical surface area, higher catalyst, volume and both axial and radial flow). Though such supports are hardly reported in the scientific literature for deN2O, e.g., thermal characteristics investigations of N2O decomposition in a catalyst igniter with metal-foam configuration for hybrid rocket propulsion system or monopropellant thruster [28]. Foams as catalyst support for deN2O are mentioned in a patent [29]. Recently, Klegova et al. [30] reported cobalt mixed oxides (Co3O4 and Co4MnAlOx) deposited on SiC open-cell foams as catalysts for deN2O (0.1 vol% N2O/N2, GHSV 3000 h−1). Catalytic activity of grain active phase was higher via Co3O4 and Co4MnAlOx prepared by suspension method than impregnation.

Due to our broad experience in preparation of HT derived catalyst and their application in deN2O [e.g. 31–33], in this study we proposed Rh-containing HT derived mixed oxides based on open-cell metallic foams as novel structured catalyst for deN2O. The coating of FeCralloy 80 ppi foams with HT compounds was performed by the electro-base generation method. This procedure was previously developed by us in order to prepare Rh-based structured catalysts dedicated for the partial oxidation of CH4 [34]. We compared the structured catalysts with materials obtained via conventional coprecipitation in terms of both physico-chemical properties and catalytic activity (conversion, reaction rate and apparent activation energy). Finally, we characterized the spent structured catalysts in order to investigate the coating stability and the nature of the active phase to give insight into property-activity relationships.

2. Experimental

A nomenclature (used abbreviations and symbol) were provided in Supplementary information (Tables S1, S2).

2.1. Catalysts preparation

Open-cell FeCralloy foams (80 ppi, panel, 7 mm thickness) were cut in cylindrical shape (diameter × height = 8 × 7 mm) and used as supports in the preparation of structured catalysts. All chemicals were purchased from Sigma Aldrich: Mg(NO3)2·6H2O (> 99%), Al (NO3)3·9H2O (> 98%), Rh(NO3)3 solution (10 wt% Rh in HNO3).

Electrosyntheses were performed in a homemade double-compartment flow electrochemical cell using a potentiostat (Autolab, PGSTAT128N, Eco Chemie) with general purpose electrochemical software (GPES). A Pt foil (0.4 mm diameter and 400 mm in length) and a saturated calomel electrode (SCE) were used as counter and reference electrode (C.E. and R.E.), respectively. Working electrode (W.E.) was the FeCralloy cylinder foam. Detailed information of the setup was reported elsewhere [34]. The electrolytes were 0.06 M aqueous solutions of the respective metal nitrates with a molar ratio (mol. ratio) of Rh/Mg/Al = 2/70/28 or 1/70/29. The potential applied for all the cases was −1.2 V vs SCE for 1500 s. After electrosynthesis, the coated foams were washed with distilled water and dried at 40 °C for 24 h. Finally, the calcination step was conducted at 600 °C for 6 h with a 10 °C min−1 heating rate. The obtained catalysts were denoted as F-Rh-2 and F-Rh-1 for Rh/Mg/Al = 2/70/28 and 1/70/29 mol. ratio, respectively.

For comparative purposes, powder catalysts were prepared by a standard coprecipitation. A 1.0 M aqueous solution of the respective metal nitrates with a molar ratio of Rh/Mg/Al = 0.25/70/29.75, 0.5/ 70/29.5, or 2/70/28, was dropped into a batch reactor containing 100 ml

of a Na2CO3 solution under vigorous stirring. The pH was controlled at 10 ± 0.2 by adding dropwise a 1.0 M aqueous solution of NaOH. The amount of Na2CO3 was calculated by charge balance of the system when a trivalent cation substituted a divalent one in the brucite structure with an excess amount of 50%. The resulting slurry was aged for 0.5 h at 60 °C under stirring, filtered and washed thoroughly with warm distilled water (60 °C). After filtration, the paste cake products were dried and subsequently calcined under the same conditions used for the foam catalysts. The catalysts were named as P-Rh-0.25, P-Rh-0.5, or P-Rh-2, where the number refers to the mol. ratio of Rh in the HT material. For catalytic tests, the powder catalysts were pelletized and a fraction of materials with particle size in range of 0.25–0.50 mm was collected and used.

2.2. Characterization techniques

Scanning electron microscopy (SEM) coupled to energy dispersive spectrometry (EDS) was performed by using an EP EVO 50 Series Instrument (EVO ZEISS) equipped with an INCA X-act Penta FET® Precision EDS microanalysis and INCA Microanalysis Suite Software (Oxford Instruments Analytical) to provide images of the spatial variation of elements in a sample. The accelerating voltage was 20 kV and the spectra were collected for 60 s. As-prepared deposited, calcined and spent coated foams were analyzed in 4–6 regions of interest to specify quality of the coating (adhesion, composition and thickness) in both strut and plate zones of the foam.

High resolution transmission electron microscopy (HRTEM) characterization was carried out by a TEM/STEM FEI TECNAI F20 micro- scope equipped with an EDS analyzer. Powder catalysts were collected by scratching the coating from the foam surface and then suspending it in ethanol under ultrasounds for 20 min. The suspension was subsequently deposited on a Cu grid with lacey quanti-foil carbon film and dried at 100 °C before doing the measurement. Selected area electron diffraction (SAED) and fast Fourier transformation (FFT) were used to determine the interplanar spacing of the crystals. Particle size distribution was processed considering around 150 particles in three different zones for each sample.

Specific surface area of the catalysts was determined by N2 ad- sorption/desorption at −196 °C. The measurements were carried out using a Micromeritics ASAP 2020 instrument. Samples (two coated foams or 0.15 g powder catalysts) were degassed under vacuum, heated up to 150 °C and maintained for 30 min before performing the measurement. The specific surface area a_s(BET) was calculated using the Brunauer-Emmett-Teller (BET) multiple-point method in the relative pressure range p/p0 from 0.05 to 0.3.

Micro-Raman measurements were performed in a Renishaw Raman Invia configured with a Leica DMLM microscope (obj. 5×, 20×, 50 ×). The available sources are an Ar+ laser (514.5 nm, Pmax = 30 mW) and a diode-laser (780.0 nm, Pmax = 300 mW). The system was equipped

with edge filters to cut Rayleigh scattering, monochromators (1800 lines/mm for Ar+ laser, and 1200 lines/mm for diode laser) and a charge-coupled device (CCD) thermoelectrically cooled (-70 °C) detector. Measurements were performed with the Ar+ Laser (514.5 nm) at power level Pout = 3 mW (10% power). Each spectrum was recorded by 4 accumulations (30 s for each).

Hydrogen temperature programmed reduction (H2-TPR) was per- formed in an AutoChem II (Chemisorption analyzer, Micromeritics). The catalyst (two coated foams or 20 mg of powder catalyst) was firstly outgassed at 150 °C under 30 ml min−1 of He for 30 min. After cooling to 30 °C under He gas, the carrier gas was switched to 5 vol% H2/Ar at 30 ml min−1. When the baseline was stable, the temperature was in- creased to 900 °C with a ramp of 10 °C min−1. The amount of H2 consumed was measured by means of a thermal conductivity detector (TCD). Water vapour was removed from effluent gas by the means of a cold trap placed in an ice-water bath.

X-ray photoelectron spectroscopy (XPS) studies were carried directly on the foam on a Physical Electronics spectrometer (PHI Versa Probe II Scanning XPS Microprobe, Physical Electronics) with mono- chromatic X-ray Al Kα radiation (100 μm, 100 W, 20 kV, 1,486.6 eV) and a dual beam charge neutralizer. The spectrometer energy scale was calibrated using Cu 2p3/2, Ag 3d5/2, and Au 4f7/2 photoelectron lines at 932.7, 368.2 and 84.0 eV, respectively. Under a constant pass energy mode at 23.5 eV condition, the Au 4f7/2 line was recorded with 0.73 eV full width at half maximum (FWHM) at a binding energy (BE) of 84.0 eV. Recorded spectra were always fitted using Gauss-Lorentz curves. Atomic concentration percentages of the characteristic elements of the surfaces were determined taking into account the corresponding area sensitivity factor for the different measured spectral regions.

2.3. Catalytic tests

The catalytic deN2O tests were performed in a quartz reactor (ID 8 mm) containing two foams of catalyst (diameter 8 mm and height 7 mm). Prior to each experiment, the structured catalysts were out- gassed at 500 °C for 0.5 h under 80 ml min−1 of N2 and then cooled down to 50 °C. After that, 80 ml min−1 of a gas mixture containing of 1000 ppm N2O in N2 was switched on to pass through the catalyst bed with gas hourly space velocity: GHSV = 6800 h−1 (or weight hour space velocity: WHSV = 480,000 L kg−1h−1 calculated based on 10 mg coating materials). The reaction was carried out at atmospheric pressure and in a range of temperatures from 50 °C to 500 °C (in absence of inhibitor) or to 600 °C (in presence of inhibitors) with an interval of 50 °C. At each temperature, the reaction was stabilized for 0.5 h before sending to quantify N2O concentration. The gas composition in the outlet stream was analyzed by infrared spectroscopy using an Agilent Cary 660 equipped with a Pike 2 m heated gas cell. The conversion of N2O (X(N2O)) was determined according to X(N2O) = ([c(N2O)in-c (N2O)out]/c(N2O)in)x100%, where: c(N2O)in and c(N2O)out – concentration of N2O in the

inlet gas, and concentration of N2O in the outlet gas. The most active catalyst was tested with 1000 ppm N2O, 200 ppm NO, 2 vol% O2 in N2 balance. The same conditions were applied for 24 h stability test at 475 °C.

DeN2O tests over pelletized powder catalysts were performed by keeping the same catalytic bed volume and the nominal amount of Rh in foams. Thus, the activity of 10 mg of P-Rh-2 was compared with the activity of 2 coated foams F-Rh-2 (also containing 10 mg Rh-2 coating). In order to keep constant catalytic bed the P-Rh-2 catalyst was diluted with MgAlOx (Mg/Al = 70/30, mol. ratio, particle size in the range of 0.25–0.50 mm). In addition, some tests were also carried out with different mass of the P-Rh-2, P-Rh-0.5, P-Rh-0.25 catalysts (10–300 mg). Apparent activation energy was calculated from the slope of linear regression derived from Arrhenius equation k = A·e−(Ea/RT), where k was calculated from kinetic model for the flow reactor with assumption of the first order reaction kτ = X(N2O)/(1-X(N2O) [35]. In which k (s−1) is reaction rate, A is pre-exponential factor, Ea (kJ mol−1) is ap- parent activation energy, R (J mol−1 K−1) is ideal gas law constant, T (K) is temperature, τ (s) is space time and X(N2O) (%) is N2O conversion. To minimize influence of heat generated from exothermic reaction as well as mass transfer issue, calculations were performed for data points with conversion lower than 30%. Except in cases with presence of inhibitors, the last point (in three-point linear regression model) with conversion higher than 30% at 450 °C were used due to lack of data points.

3. Results and Discussion

3.1. Precursor and catalyst characterization

The precipitation of a 14.5 ± 2.7 wt% solid on the surface of the foams, regardless of the Rh loading (F-Rh-2 or F-Rh-1 for Rh/Mg/ Al = 2/70/28 and 1/70/29, mol. ratio), took place during electrodepositions at −1.2 V for 1500 s. A longer time, i.e. 2000 s, partially blocked the pores of the foam support (not shown). Noted that the cell and pore size of the foam support was approximately 425 and 185 μm, respectively (Fig. S1). The high solid loading obtained (Table 1) in comparison to our previous work (i.e., 4.6 wt% [34]) could be related to the decrease in the size of the foam (from 10 mm × 11.9 mm [34] to 8.0 mm × 7.0 mm in current study). The smaller size of support may favor the effective replenishment of the solution and a more homogeneous potential distribution to achieve the desired pH value close to the foam surface. Moreover, the differences in the foam density should

Table 1

Properties of structured and powder catalysts.

Sample	Composition[a] Rh/Mg/Al (mol. ratio)	Fresh loading (wt%)	Calcined loading (wt%)	a_s(BET) (m^2 g-1) Foam[b]	Coating[c]	Pellet[d]
F-Rh-1	0.8/72.0/27.2	14.0 ± 0.7	6.7 ± 0.4	5.7	85.0	–
F-Rh-2	1.8/72.6/25.6	14.5 ± 2.7	8.4 ± 1.7	7.8	93.0	–
P-Rh-2	2.2/69.4/28.4	–	–	–	–	289.0

[a] Determined by EDS.

[b] For whole two coated foams.

[c] Only the coating.

[d] Powder catalysts prepared by co-precipitation.

be considered, i.e., a lower density means a larger wt% for the same mass of coating. Note that during the electrodepositions of F-Rh-2 and F-Rh-1 precursors, the current profiles obtained were comparable regardless of the Rh ratio in the electrolytes as shown in Fig. S2, in agreement with our previous study [34]. The coated layer was composed of spherical and platelet-like nanoparticles (Fig. 1a-a1), characteristic of electrodeposited HT compounds and similar to those of coprecipitated samples (Fig. 1b). The average Rh/Mg/Al mol. ratio in the deposits (estimated by EDS) remained close to the nominal ones, as follows: 1.8/72.6/25.6 and 0.8/72.0/27.2 for F-Rh-2 and F-Rh-1, respectively. We identified also some Mg-rich layers. In the structured catalysts (F-Rh-2 and F-Rh-1) the Rh loading was slightly lower than the nominal one. Otherwise, in the P-Rh-2 powder material, Rh loading was somewhat higher with Rh/Mg/Al = 2.2/69.4/28.4, mol. ratio.

After calcination at 600 °C for 6 h, the removal of physisorbed and intercalated H2O, hydroxyls and intercalated anions in the HT coating provoked weight loss of about 40 wt% [36], resulting in a solid loading of 8.4 ± 1.7 wt% in the F-Rh-2 structured catalyst (6.7 ± 0.4 wt% for F-Rh-1; Table 1). The thermal treatment did not largely alter the morphology of the coating and the size of the catalyst particles (Fig. 1c-c1), like for the powder sample (Fig. 1d). Despite the similarities in the morphology, materials differ in the specific surface area a_s(BET):289.0 m^2g-1 for the co-precipitated powder catalyst and 93.0 m^2 g−1 for the F-Rh-2 coated layer (85.0 m^2 g−1 for F-Rh-1, Table 1). The specific surface area for the whole coated foam reached 7.8 m^2 g−1 (considering the F-Rh-2 catalyst loading, i.e., 8.4 wt%). During calcination with applied conditions (600 °C, 6 h) no α-Al2O3 phases are expected to appear by oxidation of the

FeCralloy [37]. Instead, γ-Al2O3 could appear [38]. Furthermore, the calcination of a bare foam resulted in formation of Fe2O3 (hematite) and Fe3O4/FeCr2O4 phases [39–41], as evidenced by the bands in the Raman spectra at 297, 415, 614 and 1335 cm−1 (for Fe2O3) and 675 cm−1 (Fe3O4/FeCr2O4, Fig. S3). Besides, some carbonaceous species appeared at 1360 and 1590 cm−1. These compounds did not contribute to the specific surface area of the structured catalyst, since the adsorption/desorption of N2 in the calcined bare foam did not give any reliable isotherm data (not shown).

HRTEM characterization of the F-Rh-2 catalytic coating was dis-played in Fig. 2a and b. The sample consisted of small nanoparticles of a mixed oxide, as confirmed by SAED (inset Fig. 2a). We could not identify any Rh particles, although EDS analyses confirmed its presence

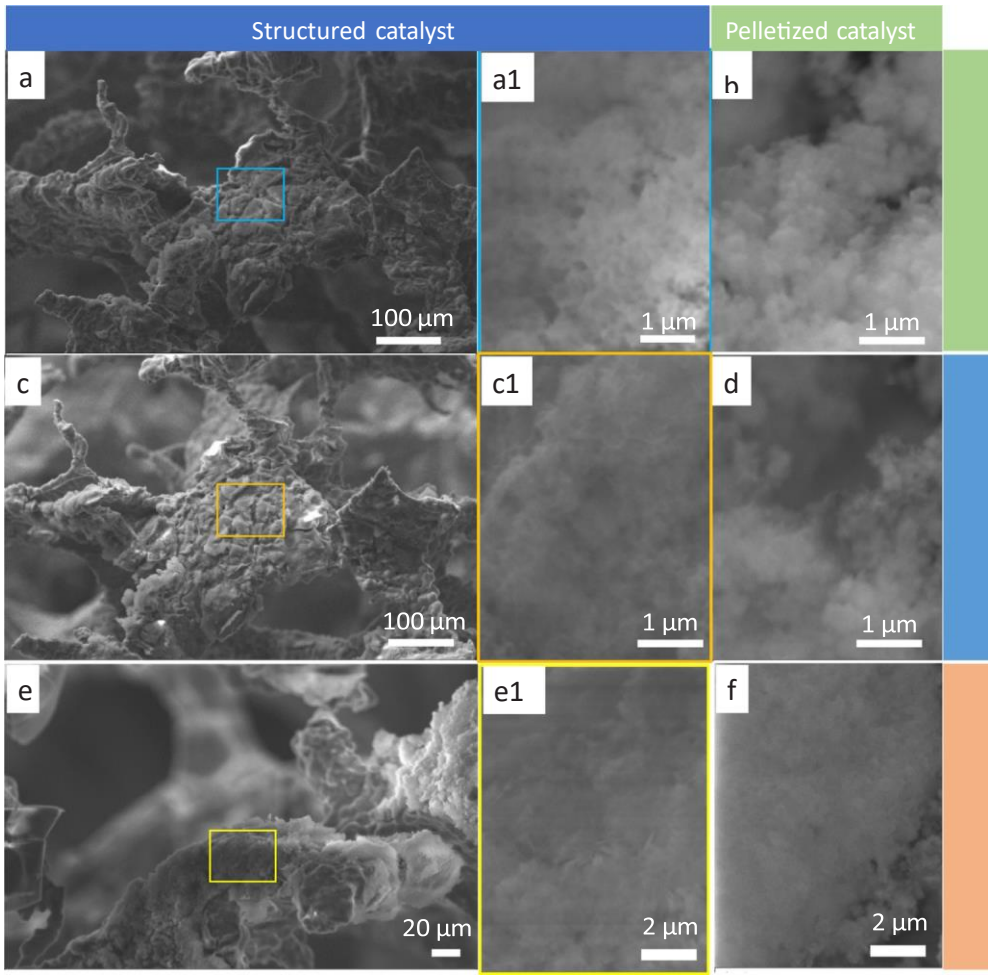

Fig. 1. SEM images of open-cell foams coated with Rh-containing HT materials (F-Rh-2): electrodeposited (a, a1), calcined sample (c, c1), spent catalyst (e, e1) and of pelletized catalyst prepared by coprecipitation (P-Rh-2): as-synthesized (b), calcined sample (d), and spent catalyst (f)

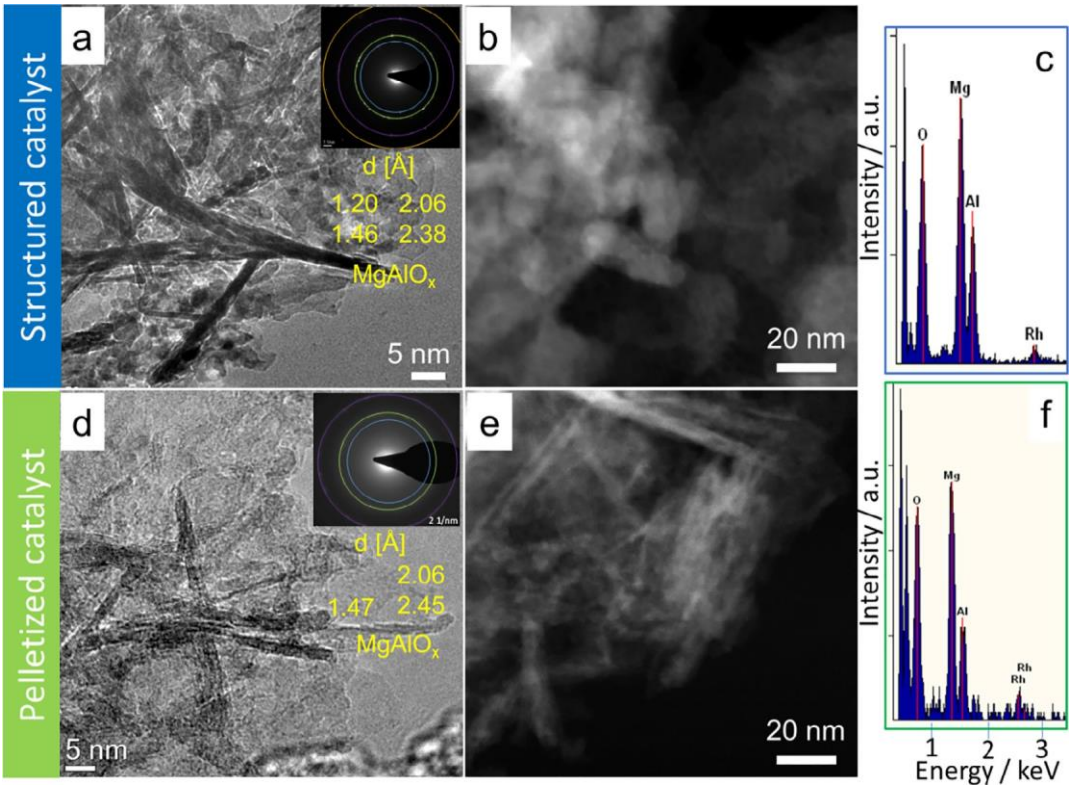

Fig. 2. TEM images of F-Rh-2 calcined catalyst: a) HRTEM; b) STEM/HAADF, c) EDS spectrum and P-Rh-2: d) HRTEM; e) STEM/HAADF, and f) EDS spectrum.

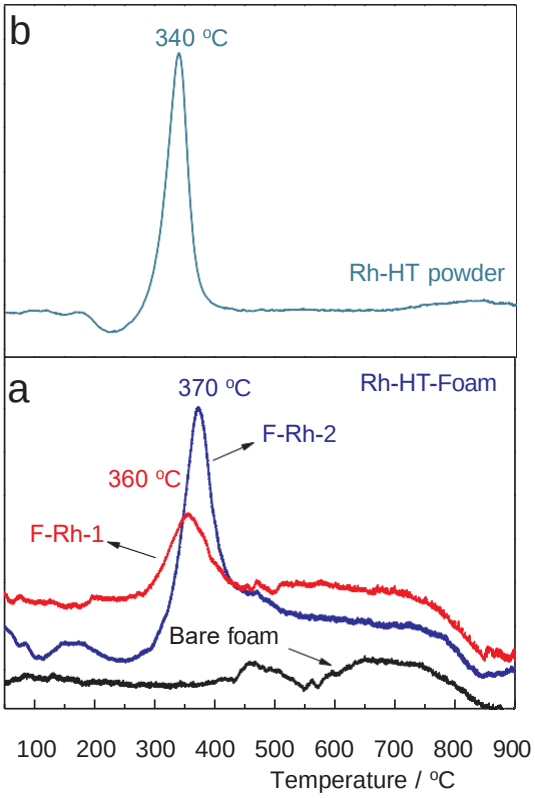

Fig. 3. H2-TPR profiles of Rh-containing structured catalysts (F-Rh-1 and F-Rh- 2) and pelletized catalyst (P-Rh-2).

(Fig. 2C). On the other hand, for the P-Rh-2 powder catalyst, regions containing both ill- and well- identified rhodium particles were observed (Fig. 2d-f). The strong interaction of Rh3+ species with the oxide matrix in the electrodeposited catalytic coating was confirmed by H2-TPR experiments. A H2 consumption peak with maximum at ca. 370 or 360 °C was recorded for F-Rh-2 and F-Rh-1 (Fig. 3a), respectively. The less intense and broad consumption at temperatures above 500 °C could be related to the reduction of the oxides developed in the foam during calcination. Indeed, a broad and low intense H2 consumption was recorded in the H2-TPR profile of the calcined bare foam. The reduction behavior of F-Rh-2 below 700 °C resembled that of the analogous P-Rh- 2 co-precipitated sample, although the latter was shifted to slightly lower temperatures, i.e. 340 °C (Fig. 3b). This behavior could be related to the specific surface area of both materials or to the Rh3+-oxide interaction.

3.2. Catalytic investigations

The bare calcined foams showed a negligible conversion of N2O at 500 °C (< 1%) (Fig. 4), despite the presence of iron oxides (as con- firmed by Raman spectroscopy in Fig. S3). Thus, the activity of the structured catalysts was related to the active phase of the coating. The activity of the structured catalysts varied for the Rh loading. The F-Rh-1 catalyst showed a 50% conversion of N2O at 380 °C (T50) with full conversion at 500 °C. On the other hand, F-Rh-2 required slightly lower temperatures for deN2O (T50 at 335 °C and full conversion at 450 °C). Two pairs of two-coated F-Rh-2 foams revealed comparable activity (Fig. 4), which allowed to confirm the reproducibility of the preparation method.

The activity of the F-Rh-2 structured catalyst was compared with the P-Rh-2 co-precipitated catalyst. The reactor volume and the nominal Rh loading were selected based on previous studies in deN2O [e.g. 6,22]. Thus, P-Rh-2 was diluted with a Mg-Al HT-derived mixed oxide (Mg70Al30) to obtain the same catalyst bed volume as for two F-Rh-2 coated foams (total amount of coating 10 mg equivalent to 6.4 μmol Rh cm−3 of catalytic bed). The activity of the diluent in deN2O was negligible up to 500 °C. To investigate if the dilution affected the catalytic activity due to bypassing and axial dispersion [42], a test was

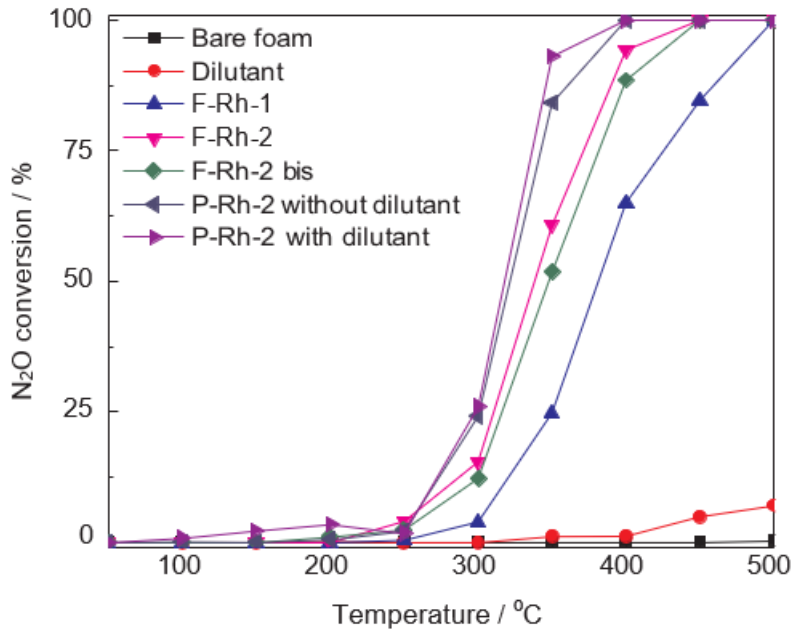

Fig. 4. Comparison of activity of structured and pelletized catalyst (Rh/Mg/Al

= 2/70/28, mol. ratio) in N2O decomposition. Reaction conditions:

80 ml min−1, 1000 ppm N2O/N2 and GHSV = 6800 h−1 (or WHSV = 480,000 L h−1 kg−1).

performed by loading the P-Rh-2 pelletized catalyst without diluent. Comparable activity was obtained for both diluted and pure P-Rh-2 catalysts (Fig. 4). The particle size of 0.25–0.50 mm of our samples used for the catalytic measurements was in the same scale order than the particle size of the samples of the study reported by Klyushina et al.[43] or Perbandt et al. [19] who reported the absence of internal and external diffusion limitations. In fact, we made a calculation to check internal diffusion limitation and found that the third characteristic dimensionless Damkȍhler number (Da-III) was around 0.029, which was still in safety zone (< 1) and hence suggested that there was no influence of internal mass transfer limitation [44]. Detail of calculation information can be found in the Supporting information. Moreover, for the reactor diameter and the catalyst bed length criteria requirement were checked. D (reactor diameter)/dp (particle diameter) ≈ 16 was above and L (catalyst bed length)/dp was in the range of 28–56. Therefore, we can certify that the catalytic reactions were performed under conditions where transport resistances are negligible [45].

The F-Rh-2 catalyst exhibited the onset temperature at 250 °C and full conversion at 450 °C, while the P-Rh-2 pelletized catalyst reached full conversion at 400 °C (Fig. 4). Note that the amount of Rh in F-Rh-2 (Rh/Mg/Al = 1.8/72.6/25.6, mol. ratio) was slightly lower than that in P-Rh-2 (Rh/Mg/Al = 2.2/69.4/28.4, mol. ratio; Table 1). The activity of structured catalyst can be further enhanced by increasing the coating thickness or the Rh loading on the coating. Electrodeposited Rh-HT structured catalyst are alkali free, while Rh-HT pellets prepared by coprecipitation may contain some traces of residual Na (though not identified by EDS analysis

of the pellets), which could influence catalytic activity [46]. Alkali metals (e.g. Na, K, Li) can act as basic centres. Furthermore, even application of similar cleaning procedure may result in varied loading of Na residual [33].

The obtained catalytic activity (Fig. 4) matched quite well with previously reported for Rh-containing HT-derived mixed oxides by Centi et al. [17] (0.1 g catalyst containing total 38.9 μmol Rh, 1 vol% N2O/He, 4 wt% Rh impregnated on Mg71Al29Ox, GHSV 1800 h−1, T50 ~ 300 °C, full conversion at 490 °C) and Oi et al. [47] (0.1 g cata- lysts containing 9.7 μmol Rh, 0.095 vol% N2O, 5 vol% O2/He, 1 wt% Rh in Rh/ZnO, total flow rate 80 ml min−1, T50 ~ 270 °C, full conversion at~325 °C). However, in our studies the catalyst amount (containing approximate total 4.5 μmol Rh) was lower from two- to eight-fold than the ones previously used. Our data therefore suggested that coating a Rh-based catalyst on the high geometrical surface area of open-cell foam could be a promising approach to decrease the use of such costly Rh-based

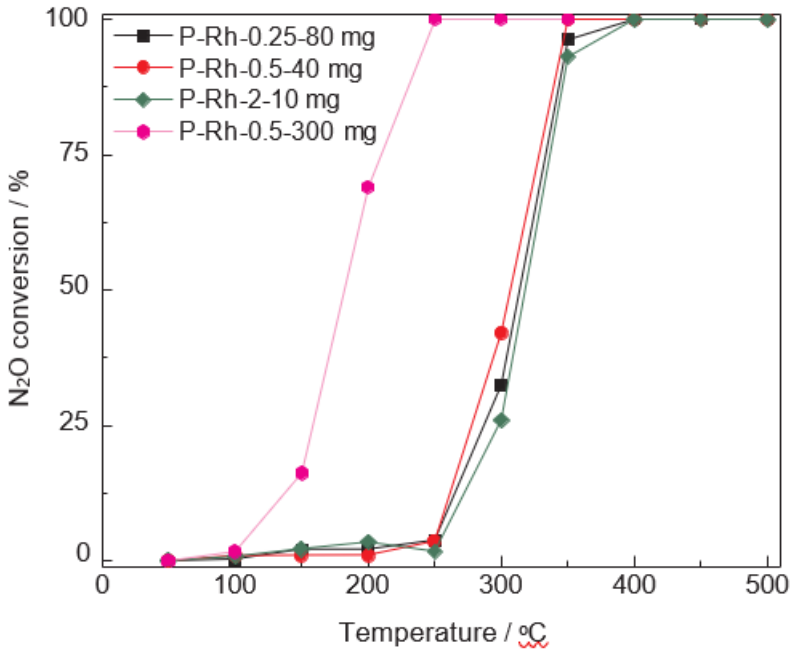

Fig. 5. Effect of Rh composition in pelletized catalysts on the activity of N2O decomposition. Reaction conditions: 80 ml min−1, 1000 ppm N2O/N2. All tests were performed at GHSV = 6800 h−1 (with dilutant for P-Rh-0.5–40 mg, and P- Rh-2–10 mg), except the test of 300 mg P-Rh-0.5 at GHSV = 1900 h−1.

materials.

One of the main advantages of Rh-containing catalysts obtained from HT precursors is the ability to prepare materials with low to high Rh loading. In the present work, to balance the low amount of catalyst deposited on the structured support (~10 mg), high loaded Rh-con-

taining HT-derived compounds were used (i.e., Rh2Mg70Al28 with a 4.6 wt% Rh). To investigate whether the high Rh loading in the catalysts could modify the catalytic activity due to differences in Rh dispersion and reducibility, deN2O tests with constant 6.4 μmol Rh cm−3 of catalytic bed were carried out over low loaded Rh0.25Mg70Al29.75 (0.6 wt% Rh) and Rh0.5Mg70Al29.5 (1.2 wt% Rh) pelletized HT-derived catalysts (P-Rh-0.25 and P-Rh-0.5, respectively). These catalysts showed comparable activity (Fig. 5). In addition, for the P-Rh-0.5 catalyst, N2O conversion increased in the temperature range up to 300 °C together with increasing the catalyst loading from 40 mg to 300 mg (Fig. 5). Thus, below 300 °C, the catalysts worked under kinetic regime [48].

The structured (F-Rh-2) and pelletized (P-Rh-2) catalysts (Fig. 6a) were also investigated in the presence of O2 and NO. The inhibitors significantly decreased catalyst activity. DeN2O curves were shifted towards higher temperatures, around 120 °C, i.e., T50 values being 455 and 440 °C for structured and pelletized catalysts, respectively. Both NO and O2 could adsorb on the active sites of the catalysts making them unavailable for N2O adsorption/activation and recombination of oxygen [17,49]. According to the generalized reaction mechanism [50,51], transition (noble) metal species as the catalytically active sites (*) can be oxidized by surface oxygen (O) species released upon deN2O (Eq. (1)) or by the adsorptive dissociation of gaseous oxygen (Eq. (2)):

$N_2O + * \rightarrow O^* + N_2$ (1)

$O_2 + 2^* \rightarrow 2O^*$ (2)

The regeneration of the active sites (removal of the surface oxygen) follows according to the Langmuir-Hinshelwood mechanism (through recombination of surface oxygen species; Eq. (3)) or according to the Eley-Rideal mechanism (through reaction between surface oxygen species and N2O; Eq. (4)):

$2O^* \rightarrow O_2 + 2^*$ (3)

$N_2O + O^* \rightarrow N_2 + O_2 + *$ (4)

Additionally, due to a slight difference in Rh content between foam catalyst (Rh/Mg/Al = 1.8/72.6/25.6, mol. ratio) and pellet (2.2/69.4/28.4, mol. ratio),

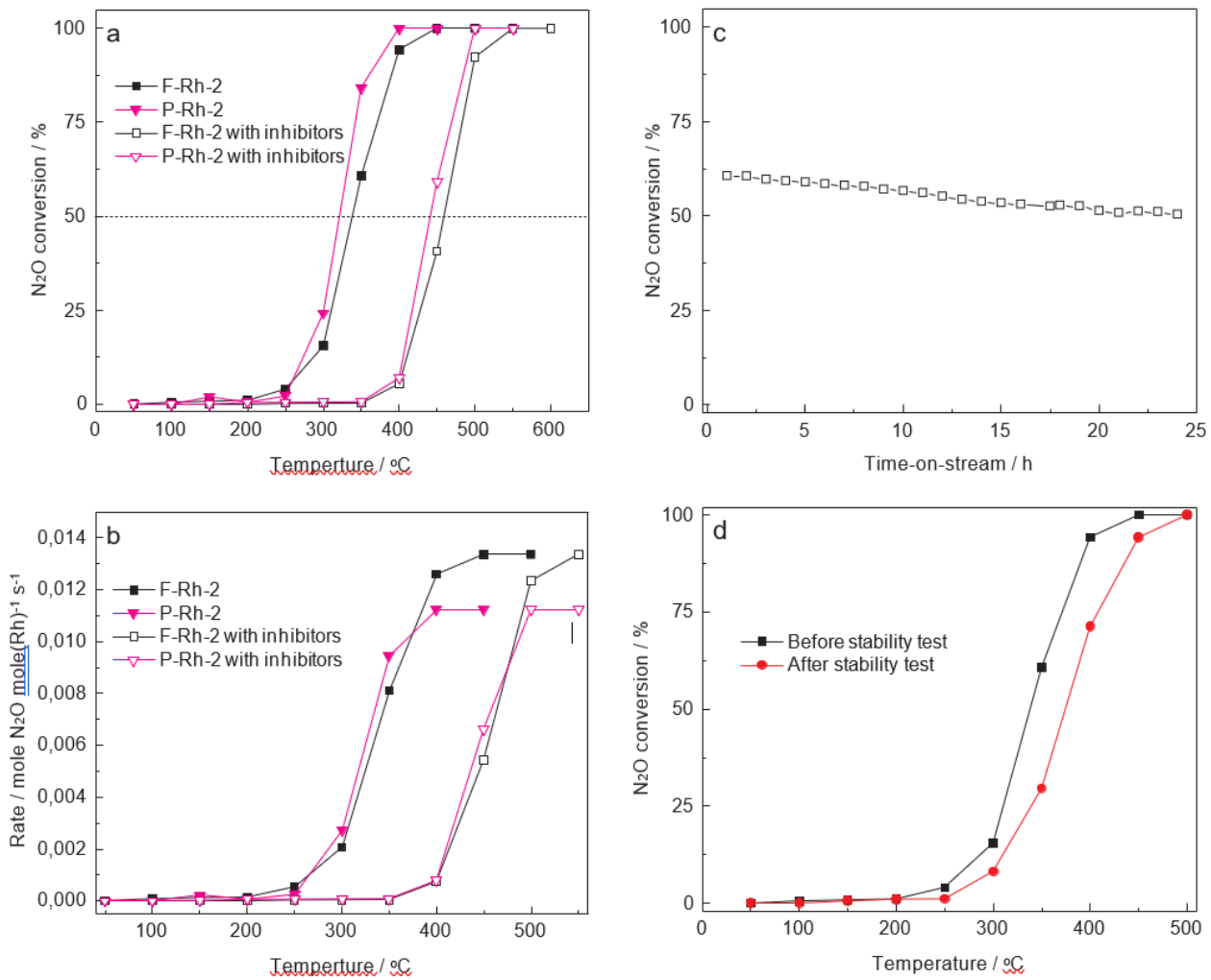

Fig. 6. Comparison of the activity of structured and pelletized catalyst in presence and absence of inhibitors (a); Stability test of F-Rh-2 structured catalyst in the presence of inhibitors at 475 °C (b), and comparison of the activity of fresh and spent structured catalyst in absence of inhibitors (c). Reaction conditions: 1000 ppm N2O/N2 (absence of inhibitors) or 1000 ppm N2O + 200 ppm NO + 2 vol% O2/N2 (presence of inhibitors), GHSV = 6800 h−1 (or WHSV = 480,000 L h−1 kg−1).

the activity performance was also compared by normalization of N2O amount (mole s−1) converted per Rh amount (mole) (Fig. 6b). Though pellet catalysts were slightly more active than the structured catalysts, the difference was not significant after normalization.

In further catalytic investigations, the same F-Rh-2 pair of foams were further applied in a long-term stability test (in the presence of O2 and NO) at 475 °C (Fig. 6c). The catalyst activity decreased with time- on-stream (TOS) from 60% to around 51% after 24 h. The deactivation rate was slightly faster in the first 20 h than that in the last 4 h. The decrease in the catalyst activity could be related to both the inhibition effect of O2 and NO already observed in Fig. 6a, and the modification of Rh species (vide infra) [52]. To verify this point, after the stability test one further trial was performed in 1000 ppm N2O/N2 (without O2 and NO in the feed) and compared with the performance of fresh catalyst (Fig. 6d). The results showed that the activity

of the spent catalyst was lower than for the fresh catalyst, confirming its partial deactivation. Thus, the physico-chemical characterization of the spent catalysts was provided.

3.3. Characterization of spent catalyst

The F-Rh-2 structured and P-Rh-2 powder catalysts (after tests carried out in the presence of O2 and NO) were further investigated in order to evaluate the changes of Rh oxidation state and particle size as well as the stability of the coating under reaction conditions (for structured catalyst). The coating in the F-Rh-2 structured spent sample was stable with no remarkable changes in morphology or sintering (Fig. 1e and e1). In addition, the specific surface area, 95.0 m^2 g−1 (8.0 m^2 g−1 for the whole coated foam) was almost similar to the value measured for the fresh material (Table 1). Since this value not only depended on the properties of the coating, but also on its amount, this further confirm the stability and adherence of the catalytic layer. HRTEM images (Fig. 7) confirmed that the morphology and size of mixed oxide particles were preserved. However, in comparison to fresh catalysts, in the spent catalysts Rh-containing nanoparticles were clearly visible potentially indicating their aggregation. In spent F-Rh-2 (after stability test in the presence of O2 and NO), a Rh-containing narrow particle size distribution in the 1–4 nm range and average size of ca. 2.0 ± 1.1 nm were measured. Similar results were obtained for the spent P-Rh-2 powder catalyst (1.3 ± 0.5 nm; catalyst measured after test in the presence of O2 and NO). Hence, from HRTEM results it could be suggested that the Rh3+ species within the mixed oxide in the calcined catalysts might be reduced under reaction conditions, resulting in the formation of observable rhodium particles (Eq. 5) [48]:

$$Rh^* - O + N_2O \rightarrow Rh^0 + N_2 + O_2 \qquad (5)$$

These Rh particles were easily identified by HRTEM. XPS analysis of the F-Rh-2 spent sample was carried out to verify the oxidation state of Rh. The Rh 3p3/2 spectrum (Fig. 8) showed two signals at 496.9 and 501.2 eV, attributed to Rh0 and Rh3+, respectively [53].

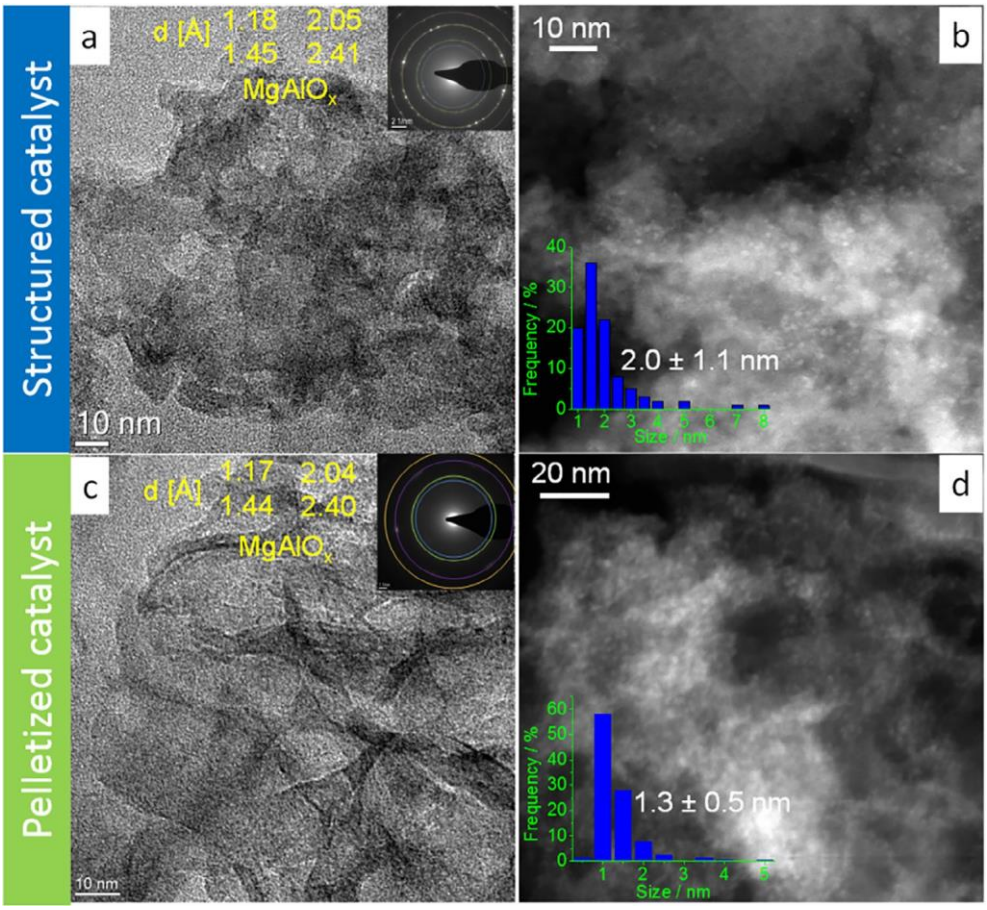

Fig. 7. TEM images of F-Rh-2 spent catalyst: HRTEM (a); STEM/HAADF (b) and P-Rh-2: HRTEM (c); STEM/HAADF (d). Insets of figure a and c are SAED while insets of Figure b and d are particle size distribution.

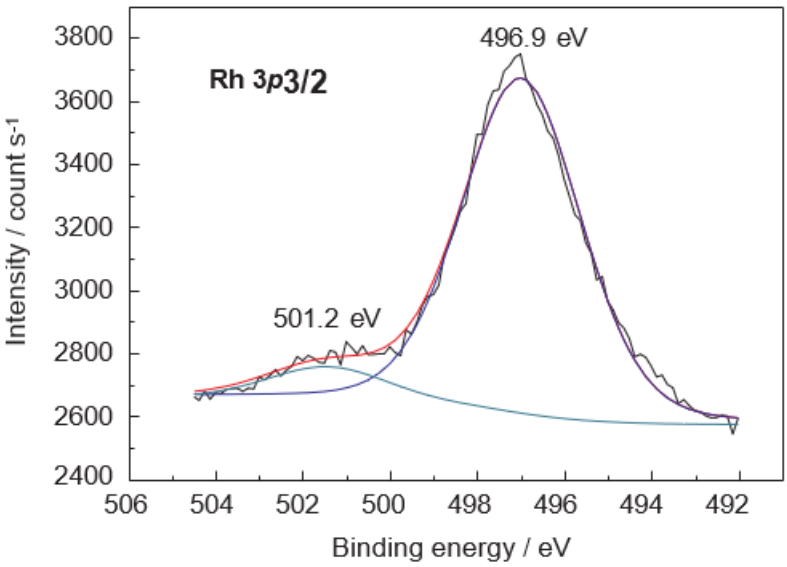

Fig. 8. XPS spectrum of Rh 3p core level obtained on F-Rh-2 spent catalyst.

The Rh^0/Rh^{3+} ratio was 11.10, thus, most of Rh^{3+} species were reduced with TOS. The coating contained only Rh^{3+} species (based on X-ray absorption near edge structure (XANES) measurements) [54]. The deactivation of the catalyst observed in Fig. 6d suggested that the partial reduction of the catalyst accompanied by a small particle size growth decreased the activity. The nature of active species, their average particle size and rhodium dispersion are essential factors for deN2O, however, were scarcely reported over Rh-containing HT derived mixed oxides. E.g. Pérez-Ramírez et al. [18] reported that these group of materials could be more active than rhodium modified alumina or zeolites (USY and ZSM-5). While, the results of activity confirmed that the higher Rh dispersion (determined by CO chemisorption) caused a higher N2O conversion. Alini et al. [11] studied H2-reduced Mg-Rh-Al-Ox (Mg/Rh/ Al = 71.0/0.5/28.5, 71.0/1.0/28.0 or 80.0/1.0/19.0, mol. ratio), and found homogeneously dispersed Rh^0 with an average particle size in the range between 1.0 and 3.0 nm as the active species for deN2O. Reoxidation of metallic rhodium during deN2O leads to lower activity, while a reheating of the catalyst in reducing atmosphere recovered its preliminary activity. Other reports indicated that, the actual active species of rhodium could depend on catalyst composition, its preparation and pretreatment strategies, etc. For example, Rh^0 as active rhodium species for deN2O over Rh/SrAl2O3 [13], while Rh^{3+} served as the active species in Rh/CeO2 [8]. Other researchers, such as Haber et al. [46] and Oi et al. [55], reported that both Rh^0 and Rh^{3+} were active for deN2O, etc. Besides, the rhodium oxidation state, also the Rh particle size plays a vital role for high catalytic deN2O performance. Most of the researchers agree, that the smaller the rhodium size the higher the catalytic activity in deN2O. E.g. Rh/Al2O3 with an average particle size of 1.86 nm revealed complete deN2O at a temperature of about 100 °C higher than Rh/SrAl2O3 (average particle size of 1.20 nm) [13]. On the other side, there are studies reporting enhanced activity over relatively large rhodium particles (2.1–2.4 nm) [6]. Thus, further studies over individual catalytic system remain necessary to elucidate the size, distribution, shape and degree of agglomeration of the metal/oxide particles.

3.4. Apparent activation energies and reaction rates

Arrhenius plots for both structured and pelletized catalysts were calculated in the

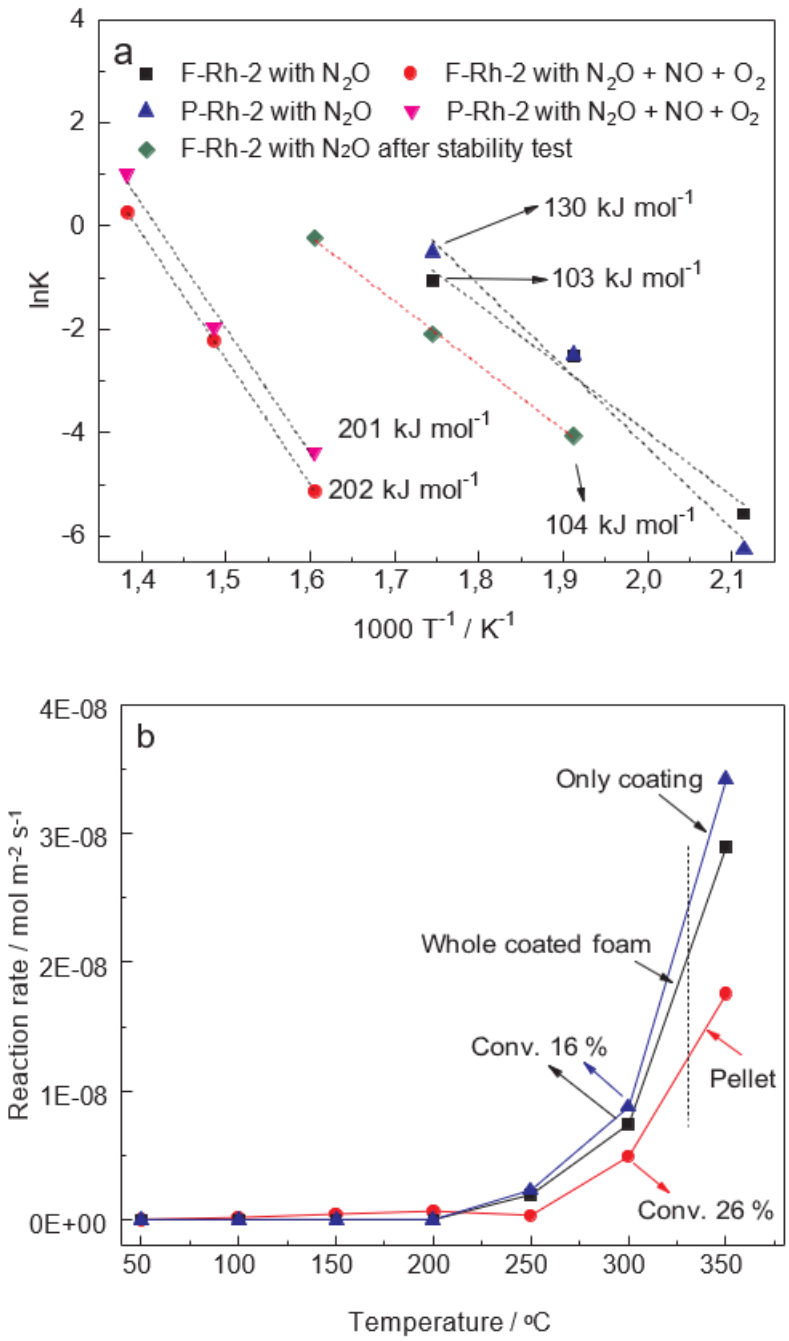

Fig. 9. Comparison of structured and pelletized catalysts: Arrhenius plots for calculation of apparent activation energy (a) and reaction rate (b). Note that reaction rate for sole coating was calculated based on mass of only the coating and its specific surface area of 95 m^2 g−1.

temperature range of 200–300 °C and 350–450 °C in absence and presence of inhibitors, respectively, assuming a pseudo first order kinetics (Fig. 9a). The apparent activation energies for F-Rh- 2 and P-Rh-2 were 103 and 130 kJ mol−1 in absence of inhibitors, respectively. A lower activation energy for F-Rh-2 (200–300 °C) resulted in a higher reaction rate, as shown in Fig. 9b. For example, the F-Rh-2 structured catalyst exhibited 6-fold and 1.5-fold higher reaction rates than the P-Rh-2 pelletized catalyst at 250 and 300 °C, respectively.

Furthermore, this ratio was even slightly higher when comparing with sole coating. Note that reaction rate of sole coating was calculated based on specific surface area and mass of only the coating, which were different from those calculated for the whole foam catalyst. The reaction rate and activation energy were well correlated with the catalyst reducibility since Rh^{3+} in F-Rh-2 was more stable than that in P-Rh-2 (according to the H2-TPR profiles; Fig. 3). The activation energy of P- Rh-2 catalyst is quite close to that on Rh/γ-Al_2O_3 reported in the scientific literature [48,56], and hence may indicate similar reaction mechanism for P-Rh-2 tested in our studies. Rhodium on Rh/γ-Al_2O_3 is reduced to Rh^0 under reaction conditions and N_2O decomposition over catalysts may occur via the Eley-Rideal mechanism (successive oxidation and reduction of rhodium species by N_2O) [56].

In presence of both O_2 and NO, the apparent activation energy value increased to 202 and 201 kJ mol^{-1} for structured and pelletized catalysts, respectively. The increase of apparent activation energy suggested that O_2 present in the feed stream favors regeneration of the active sites via Eley-Rideal mechanism (Eq. (4)) [57]. The apparent activation energy for the spent catalyst after stability test was about 104 kJ mol^{-1}, almost the same for the fresh F-Rh-2 catalyst (103 kJ mol^{-1}). Thus, the reaction mechanism is similar in both cases, regardless contribution of Rh^{3+} and Rh^0 in the fresh and spent samples. Finally, we compared the performances of the catalysts studied in this work with previously reported, in terms of the amount of N_2O converted per amount of Rh (mol N_2O h^{-1} mol Rh^{-1}) at T50. Table S3 summarizes the values obtained for F-Rh-2 (very similar to P-Rh-2) and selected catalyst, including: Rh supported on Al_2O_3, SiO_2, TiO_2, hydroxyapatite, ZnO, CeO_2, ZSM-5, as well as honeycomb monolith. Discussion of activity over other Rh-containing catalysts can be found in our previous review [5]. Though it is challenging to make accurate comparisons due to differences in reaction conditions, it could be stated that our catalysts (having a value of 22 and 44 mol(N_2O) h^{-1} mol $(Rh)^{-1}$) are in line with previously reported catalysts (also in the ranges of temperatures). The activity of the structured catalysts could be further enhanced by tailoring the Rh-HT composition and the catalyst mass in the structured reactor [14,58,59]. The latter could be performed either by modifying the pore size, coating thickness or increasing the bed length. As shown for the P-Rh-0.5 powder catalyst, light-off and full conversion temperatures could be shifted to 150 and 250 °C, by doubling the Rh loading ~35 μmol Rh 2.5 cm^{-3} (14 μmol Rh cm^{-3} catalytic bed) (Fig. 5). Also, a true evaluation of the economic potential of our system would require further investigations under different reaction conditions concerning the activity, selectivity and stability of this material (catalytic tests in the presence of NO, O_2, water vapor; variation of GHSV). However, at this stage, such measurements were not carried out, and are planned for further studies over optimized catalysts based on open-cell metallic foams. Furthermore, such alter- native-type catalysts will be compared with industrially relevant transition metal-containing system in terms of their activity, selectivity and stability.

4. Conclusions

Open-cell metallic foams are alternative 3D supports to honeycomb monoliths for the deN2O reaction. The coating of the foams by electrodeposition of Rh/Mg/Al HT compounds can provide a loading of ca. 17 mg 0.7 cm−3 foam. After calcination at moderate temperatures, i.e., 600 °C, HT compounds were transformed into structured catalysts. Such materials revealed properties similar to powder catalysts (prepared by conventional co-precipitation) in terms of morphology, crystallinity and Rh particle size. Both materials varied slightly for their textural and redox properties, and consequently in deN2O performance. The F-Rh-2 structured catalyst exhibited the onset temperature at 250 °C and full conversion at 450 °C, while the P-Rh-2 pelletized catalyst reached full conversion at 400 °C. Furthermore, rhodium oxides were reduced to Rh0 with TOS over the F-Rh-2 catalyst, while the coating remained stable without detaching and modifications on the textural and structural properties of the MgAlOx mixed oxide support. The mass of the coating on the foam (6.7 ± 0.4 versus 8.4 ± 1.7) significantly determined the catalyst activity (full conversion at 500 °C versus 450 °C). However, the ability to tailor the Rh loading (by increasing the coating thickness or the Rh loading on the coating) in the original HT structure opens new possibilities to improve the activity of structured catalysts. Hence, the integration of Rh-HT-derived material on open-cell metallic foam may provide promising structured catalysts for catalytic decomposition of N2O in terms of catalyst efficiency and process intensification, decreasing pressure drop.

Acknowledgements

P.H. Ho thanks to SINCHEM grant for PhD research fellowship.

SINCHEM is a joint-doctorate program selected under Erasmus Mundus Action 1 program (FPA 2013-0037).

E.R.C. thanks to Ministerio de Ciencia, Innovación y Universidades of Spain (project RTI2018-099668-B-C22) and FEDER Funds.

M.J. and R.P. thank to the Excellence Initiative of the German Federal and State Governments in the frame of the Center for Automotive Catalytic Systems Aachen (ACA) at RWTH Aachen University.

References

[1] M. Strokal, C. Kroeze, Nitrous oxide (N2O) emissions from human waste in 1970–2050, Curr. Opin. Environ. Sustain. 9–10 (2014) 108–121.

[2] B.A. Hungate, J.S. Dukes, M.R. Shaw, Y. Luo, C.B. Field, Nitrogen and climate change, Science 302 (2003) 1512–1513.

[3] A.R. Ravishankara, J.S. Daniel, R.W. Portmann, Nitrous Oxide (N2O): the dominant ozone-depleting substance emitted in the 21st century, Science 326 (2009)

123–125.

[4] M. Konsolakis, Recent Advances on Nitrous Oxide (N2O) Decomposition over non-noble-metal oxide catalysts: catalytic performance, mechanistic considerations, and surface chemistry aspects, ACS Catal. 5 (2015) 6397–6421.

[5] M. Jabłońska, R. Palkovits, It is no laughing matter: nitrous oxide formation in diesel engines and advances in its abatement over rhodium-based catalysts, Catal. Sci. Technol. 6 (2016) 7671–7687.

[6] H. Beyer, J. Emmerich, K. Chatziapostolou, K. Köhler, Decomposition of nitrous oxide by rhodium catalysts: effect of rhodium particle size and metal oxide support, Appl. Catal. A Gen. 391 (2011) 411–416.

[7] M. Piumetti, M. Hussain, D. Fino, N. Russo, Mesoporous silica supported Rh cata- lysts for high concentration N2O decomposition, Appl. Catal. B Environ. 165 (2015) 158–168.

[8] A. Bueno-López, I. Such-Basáñez, C. Salinas-Martínez de Lecea, Stabilization of active Rh2O3 species for catalytic decomposition of N2O on La-, Pr-doped CeO2, J. Catal. 244 (2006) 102–112.

[9] E.V. Kondratenko, R. Kraehnert, J. Radnik, M. Baerns, J. Pérez-Ramírez, Distinct activity and time-on-stream behavior of pure Pt and Rh metals and Pt–Rh alloys in the high-temperature N2O decomposition, Appl. Catal. A Gen. 298 (2006) 73–79.

[10] M. Hussain, D. Fino, N. Russo, Development of modified KIT-6 and SBA-15-sphe- rical supported Rh catalysts for N2O abatement: from powder to monolith sup- ported catalysts, Chem. Eng. J. 238 (2014) 198–205.

[11] S. Alini, F. Basile, A. Bologna, T. Montanari, A. Vaccari, Preparation of stable cat- alysts for N2O decomposition under industrial conditions, Stud. Surf. Sci. Catal. 143 (2000) 131–139.

[12] C. Huang, Z. Ma, P. Xie, Y. Yue, W. Hua, Z. Gao, Hydroxyapatite-supported rhodium catalysts for N2O decomposition, J. Mol. Catal. A: Chem. 400 (2015) 90–94.

[13] S. Parres-Esclapez, F.E. López-Suárez, A. Bueno-López, M.J. Illán-Gómez, B. Ura,

J. Trawczynski, Rh–Sr/Al2O3 catalyst for N2O decomposition in the presence of O2, Top. Catal. 52 (2009) 1832–1836.

[14] M.J. Kim, Y.J. Kim, S.J. Lee, I.S. Ryu, H.J. Kim, Y. Kim, C.H. Kim, S.G. Jeon,

Enhanced catalytic activity of the Rh/γ-Al2O3 pellet catalyst for N2O decomposition using high Rh dispersion induced by citric acid, Chem. Eng. Res. Des. 141 (2019) 455–463.

[15] S.S. Kim, S.J. Lee, S.C. Hong, Effect of CeO2 addition to Rh/Al2O3 catalyst on N2O decomposition, Chem. Eng. J. 169 (2011) 173–179.

[16] V. Rico-Pérez, C. Salinas-Martínez de Lecea, A. Bueno-López, Preparation of RhOx/CeyPr1−yO2 N2O decomposition catalysts by rhodium nitrate impregnation with different solvents, Appl. Catal. A Gen. 472 (2014) 134–142.

[17] G. Centi, A. Galli, B. Montanari, S. Perathoner, A. Vaccari, Catalytic decomposition of N2O over noble and transition metal containing oxides and zeolites. Role of some variables on reactivity, Catal. Today 35 (1997) 113–120.

[18] J. Pérez-Ramírez, F. Kapteijn, X.Xu. Guido Mul, J.A. Moulijn, Ex-framework FeZSM- 5 for control of N2O in tail-gases, Catal. Today 76 (2002) 55–74.

[19] C. Perbandt, V. Bacher, M. Groves, M. Schwefer, R. Siefert, T. Turek, Kinetics and reactor design for N2O decomposition in the EnviNOx® process, Chem. Ing. Tech. 85 (2013) 705–709.

[20] T. Zhou, L. Li, C. Jie, Q. Shen, Q. Xie, Z. Hao, Fe-mordenite/cordierite monolith for the catalytic decomposition of nitrous oxide, Ceram. Int. 35 (2009) 3097–3101.

[21] R. Zhang, K. Hedjazi, B. Chen, Y. Li, Z. Lei, N. Liu, M(Fe, Co)-BEA washcoated honeycomb cordierite for N2O direct decomposition, Catal. Today 273 (2016) 273–285.

[22] V. Rico-Perez, S. Parres-Esclapez, M.J. Illan-Gomez, C. Salinas-Martinez de Lecea,

A. Bueno-Lopez, Preparation characterisation and N2O decomposition activity of honeycomb monolith-supported Rh/Ce0.9Pr0.1O2 catalysts, Appl. Catal. B Environ. 107 (2011) 18–25.

[23] G. Grzybek, P. Stelmachowski, P. Indyka, M. Inger, M. Wilk, A. Kotarba, Z. Sojka, Cobalt–zinc spinel dispersed over cordierite monoliths for catalytic N2O abatement from nitric acid plants, Catal. Today 257 (2015) 93–97.

[24] K. Jirátová, J. Balabánová, F. Kovanda, A. Klegová, L. Obalová, R. Fajgar, Cobalt oxides supported over ceria–zirconia coated cordierite monoliths as catalysts for deep oxidation of ethanol and N2O decomposition, Catal. Lett. 147 (2017)

1379–1391.

[25] S. Kumar, A. Vinu, J. Subrt, S. Bakardjieva, S. Rayalu, Y. Teraoka, N. Labhsetwar, Catalytic N2O decomposition on Pr0.8Ba0.2MnO3 type perovskite catalyst for in- dustrial emission control, Catal. Today 198 (2012) 125–132.

[26] B. Bromley, V. Hessel, A. Renken, L. Kiwi-Minsker, “Sandwich Reactor” for heterogeneous catalytic processes: N2O decomposition as a case study, Chem. Eng. Technol. 31 (2008) 1162–1169.

[27] L. del Río, G. Marbán, Stainless steel wire mesh-supported potassium-doped cobalt oxide catalysts for the catalytic decomposition of nitrous oxide, Appl. Catal. B Environ. 126 (2012) 39–46.

[28] W.J. You, H.J. Moon, S.P. Jang, J.K. Kim, Thermal characteristics of an N2O cata- lytic igniter with metal foam for hybrid rocket motors, Int. J. Heat Mass Transf. 66 (2013) 101–110.

[29] U. Jantsch, J. Lund, M. Gorywoda, M. Kraus, Catalyst for the decomposition of N2O in the Ostwald, Patent US, 2009, 20090130010 A1.

[30] A. Klegova, A. Inayat, P. Indyka, J. Gryboś, Z. Sojka, K. Pacultová, W. Schwieger,

A. Volodarskaja, P. Kuśtrowski, A. Rokicińska, D. Fridrichová, L. Obalová, Cobalt mixed oxides deposited on the SiC open-cell foams for nitrous oxide decomposition, Appl. Catal. B Environ. 255 (2019) 117745.

[31] M. Jabłońska, L. Buselli, M. Nocuń, R. Palkovits, Silver-doped cobalt (magnesium) aluminum mixed metal oxides as potential catalysts for nitrous oxide decomposi-

tion, ChemCatChem 10 (2018) 296–304.

[32] M. Jabłońska, M. Agote Arán, A.M. Beale, K. Góra-Marek, G. Delahay, C. Petitto,

K. Pacultová, R. Palkovits, Catalytic decomposition of N2O over Cu–Al–Ox mixed metal oxides, RSC Adv. 9 (2019) 3979–3986.

[33] M. Jabłońska, M. Agote Arán, G. Delahay, C. Petitto, M. Nocuń, R. Palkovits, Understanding the origins of N2O decomposition activity in Mn(Fe)CoAlOx hydro- talcite derived mixed metal oxides, Appl. Catal. B: Environ. 243 (2019) 66–75.

[34] P.H. Ho, W. de Nolf, F. Ospitali, A. Gondolini, G. Fornasari, E. Scavetta, D. Tonelli,

A. Vaccari, P. Benito, Coprecipitated-like hydrotalcite-derived coatings on open-cell metallic foams by electrodeposition: Rh nanoparticles on oxide layers stable under harsh reaction conditions, Appl. Catal. A Gen. 560 (2018) 12–20.

[35] P. Stelmachowski, G. Maniak, J. Kaczmarczyk, F. Zasada, W. Piskorz, A. Kotarba,

Z. Sojka, Mg and Al substituted cobalt spinels as catalysts for low temperature deN2O—Evidence for octahedral cobalt active sites, Appl. Catal. B Environ. 146 (2014) 105–111.

[36] F. Basile, P. Benito, G. Fornasari, V. Rosetti, E. Scavetta, D. Tonelli, A. Vaccari, Electrochemical synthesis of novel structured catalysts for H2 production, Appl. Catal. B Environ. 91 (2009) 563–572.

[37] L. Giani, C. Cristiani, G. Groppi, E. Tronconi, Washcoating method for Pd/γ-Al2O3 deposition on metallic foams, Appl. Catal. B Environ. 62 (2006) 121–131.

[38] P. Benito, W. de Nolf, G. Nuyts, M. Monti, G. Fornasari, F. Basile, K. Janssens,

F. Ospitali, E. Scavetta, D. Tonelli, A. Vaccari, Role of coating-metallic support interaction in the properties of electrosynthesized Rh-based structured catalysts, ACS Catal. 4 (2014) 3779–3790.

[39] D.L.A. de Faria, S. Venâncio Silva, M.T. de Oliveira, Raman microspectroscopy of some iron oxides and oxyhydroxides, J. Raman Spectrosc. 28 (1997) 873–878.

[40] D.L.A. de Faria, F.N. Lopes, Heated goethite and natural hematite: can Raman spectroscopy be used to differentiate them? Vib. Spectrosc. 45 (2007) 117–121.

[41] C. Cionea, M.D. Abad, Y. Aussat, D. Frazer, A.J. Gubser, P. Hosemann, Oxide scale formation on 316L and FeCrAl steels exposed to oxygen controlled static LBE at temperatures up to 800 °C, Sol. Energy Mater. Sol. Cells 144 (2016) 235–246.

[42] R.J. Berger, J. Pérez-Ramírez, F. Kapteijn, J.A. Moulijn, Catalyst performance testing: the influence of catalyst bed dilution on the conversion observed, Chem. Eng. J. 90 (2002) 173–183.

[43] A. Klyushina, K. Pacultová, K. Karásková, K. Jirátová, M. Ritz, D. Fridrichová,

A. Volodarskaja, L. Obalová, Effect of preparation method on catalytic properties of Co-Mn-Al mixed oxides for N2O decomposition, J. Mol. Catal. A: Chem. 425 (2016) 237–247.

[44] S. Wójcik, G. Ercolino, M. Gajewska, C.W.M. Quintero, S. Specchia, A. Kotarba, Robust Co3O4|α-Al2O3|cordierite structured catalyst for N2O abatement – Validation of the SCS method for active phase synthesis and deposition, Chem. Eng.

J. (2018), https://doi.org/10.1016/j.cej.2018.10.025.

[45] C. Perego, S. Peratello, Experimental methods in catalytic kinetics, Catal. Today 52 (1999) 133–145.

[46] J. Haber, M. Nattich, T. Machej, Alkali-metal promoted rhodium-on-alumina cat- alysts for nitrous oxide decomposition, Appl. Catal. B Environ. 77 (2008) 278–283.

[47] J. Oi, A. Obuchi, A. Ogata, H. Yagita, G. Bamwenda, K. Mizuno, Catalytic decom- position of N2O over rhodium-loaded metal oxides, Chem. Lett. 453–454 (1995).

[48] S. Parres-Esclapez, I. Such-Basañez, M.J. Illán-Gómez, C. Salinas-Martínez de Lecea,

A. Bueno-López, Study by isotopic gases and in situ spectroscopies (DRIFTS, XPS and Raman) of the N2O decomposition mechanism on Rh/CeO2 and Rh/γ-Al2O3 cata- lysts, J. Catal. 276 (2010) 390–401.

[49] J.A.Z. Pieterse, G. Mul, I. Melian-Cabrera, R.W. van den Brink, Synergy between metals in bimetallic zeolite supported catalyst for NO-promoted N2O decomposi- tion, Catal. Lett. 99 (2005) 41–44.

[50] L. Obalová, K. Jirátová, F. Kovanda, M. Valášková, J. Balabánová, K. Pacultová, Structure–activity relationship in the N2O decomposition over Ni-(Mg)-Al and Ni- (Mg)-Mn

mixed oxides prepared from hydrotalcite-like precursors, J. Mol. Catal. A: Chem. 248 (2006) 210–219.

[51] L. Obalová, V. Fíla, Kinetic analysis of N2O decomposition over calcined hydrotalcites, Appl. Catal. B Environ. 70 (2007) 353–359.

[52] S. Suárez, M. Yates, A.L. Petre, J.A. Martín, P. Avila, J. Blanco, Development of a new Rh/TiO2–sepiolite monolithic catalyst for N2O decomposition, Appl. Catal. B Environ. 64 (2006) 302–311.

[53] D. Briggs, M. Seah, Practical Surface Analysis by Auger and X-ray Photoemission Spectroscopies, John Wiley, New York, 1983.

[54] P. Benito, G. Nuyts, M. Monti, W.D. Nolf, G. Fornasari, K. Janssens, E. Scavetta,

A. Vaccari, Stable Rh particles in hydrotalcite-derived catalysts coated on FeCrAlloy foams by electrosynthesis, Appl. Catal. B: Environ. 179 (2015) 321–332.

[55] J. Oi, A. Obuchi, G.R. Bamwenda, A. Ogata, H. Yagita, S. Kushiyama, K. Mizuno, Decomposition of nitrous oxide over supported rhodium catalysts and dependency on feed gas composition, Appl. Catal. B: Environ. 12 (1997) 277–286.

[56] S. Parres-Esclapez, M.J. Illán-Gómez, C. Salinas-Martínezde Lecea, A. Bueno-López, On the importance of the catalyst redox properties in the N2O decomposition over alumina and ceria supported Rh, Pd and Pt, Appl. Catal. B: Environ. 96 (2010) 370–378.

[57] H. Yu, X. Wang, Apparent activation energies and reaction rates of N2O decomposition via different routes over Co3O4, Catal. Commun. 106 (2018) 40–43.

[58] M. Hussain, D. Fino, N. Russo, N2O decomposition by mesoporous silica supported Rh catalysts, J. Hazard. Mater. 211–212 (2012) 255–265.

[59] L. Chmielarz, P. Kuśtrowski, M. Drozdek, M. Rutkowska, R. Dziembaj, M. Michalik, P. Cool, E.F. Vansant, SBA-15 mesoporous silica modified with rhodium by MDD method and its catalytic role for N2O decomposition reaction, J. Porous Mat. 18 (2011) 483–491.